Interplay of local polarization, ionic size, and octahedral tilt in $SrTiO_3$-$Na_{0.5}Bi_{0.5}TiO_3$

Deepak Sharma,[1] Pooja Punetha,[1] Gobinda Das Adhikary,[1] Maxim Avdeev,[2,3] and Rajeev Ranjan[1,*]

[1]*Department of Materials Engineering, Indian Institute of Science, Bangalore 560012, India*

[2]*ANSTO, New Illawarra Rd, Lucas Heights, New South Wales 2234, Australia*

[3]*School of Chemistry, The University of Sydney, Sydney 2006, Australia*

(Received 11 July 2023; revised 27 November 2023; accepted 11 January 2024; published 30 January 2024)

We show that the ferroelectric system $(1-x)SrTiO_3$-$(x)Na_{0.5}Bi_{0.5}TiO_3$ exhibits an interesting interplay of local polarization, ionic size effect, and octahedral tilt. This interplay results in (i) a nonmonotonic composition dependence of the lattice volume at room temperature and (ii) existence of a unique temperature (300 °C) at which the competing effects of electrostriction caused by the formation of polar nanoregions and geometrical ionic size make the system exhibit composition independent lattice parameters in a large composition interval $x < 0.40$.

DOI: 10.1103/PhysRevB.109.014107

I. INTRODUCTION

For decades $SrTiO_3$ (ST) has been a model system for understanding soft mode driven structural phase transitions in crystalline solids [1]. ST is also known for its quantum paraelectric/incipient ferroelectric behavior [2]. Compared to normal ferroelectrics such as the $PbTiO_3$, wherein the frequency of the zone-center ($q = 0,0,0$) soft ferroelectric mode decreases on cooling in the paraelectric state and freezes at the Curie point, the freezing of the ferroelectric mode is precluded in ST by the overwhelming effects of quantum fluctuations associated with the zero-point vibrations [2]. The temperature dependence of permittivity of ST deviates from the classical Curie-Weiss law and, instead, follows Barrett's equation [3] which incorporates quantum corrections to the Curie-Weiss formula. The permittivity becomes almost temperature independent in the low temperature regime for such materials. The quantum fluctuations in ST can be suppressed by suitable doping and the system can exhibit quantum ferroelectric behavior for low concentration of the dopants [4–6].

Apart from the intriguing polar behavior, ST also has a soft zone boundary mode ($q = 0.5, 0.5, 0.5$). This mode freezes at 105 K leading to a cubic ($Pm\bar{3}m$)–tetragonal ($I4/mcm$) structural phase transformation [7]. This tetragonal structure is nonferroelectric and comprises of $a^0\,a^0\,c^-$ octahedral tilt [8]. The existence of the polar and nonpolar structural modes provide an interesting opportunity to tune the functionality of $SrTiO_3$ by promoting/suppressing one or the other. For example, epitaxially grown ST on a suitable substrate can stabilize the ferroelectric state even at room temperature [9]. Among the different approaches to tune the functionality of materials, chemical modification is most popular. The effect of homovalent (Ba, Ca, Pb substitutions at the Sr site) [2,10–13] and heterovalent (Pr, Bi substitutions at the Sr site) chemical modifications [14–20] on the structural and polar states of ST have been investigated in the past. Ca-modified $SrTiO_3$ i.e., $Sr_{1-x}Ca_xTiO_3$, is among the most investigated systems [4,21–26]. In the low concentration regime ($x < 0.02$), it exhibits the quantum ferroelectric ground state [4]; the dielectric maximum temperature follows $(x - x_C)^{0.5}$ composition dependence. In the higher concentration regime ($0.15 < x < 0.40$), the ground state is reported to be antiferroelectric [26]. The antiferroelectric phase (space group *Pbcm*) consists of complex modulation of the in-phase and antiphase octahedral tilt leading to quadrupling of the unit cell along the cubic axis [27]. Among the heterovalent substituents Duran *et al.* reported that Pr doping of ST stabilizes the ferroelectric phase even at room temperature [16]. The onset of a spontaneous electrostrictive strain below 500 K was also reported, supporting the development of ferroelectric correlations in Pr modified ST [18–20]. Chen *et al.* reported quantum ferroelectric and relaxor behavior below 50 K in Bi-modified ST [6].

In perovskite-based compounds, the $6s^2$ lone pair electrons of Bi^{+3} on the *A* site promote ferroelectric distortion [28]. However, the nonstoichiometric nature of the standalone Bi substitution at the Sr site limits its dissolution in ST [14,15]. A way to increase Bi concentration in the ST matrix is by alloying ST with stable Bi-based perovskite compounds such as $BiFeO_3$ (BF), $Na_{0.5}Bi_{0.5}TiO_3$ (NBT), or $K_{0.5}Bi_{0.5}TiO_3$ (KBT). The multivalent states of Fe in solids generally increase the leakage current and preclude switching of the ferroelectric-ferroelastic domains in BF-based perovskites [29]. In contrast, NBT and KBT are very good electrical insulators. Alloying ST with them can not only increase the population of Bi at the Sr site but also retain the good electrical insulating behavior of the material and allow exploitation of the functionalities associated with the mobility of domains for practical applications.

NBT is a nonergodic relaxor ferroelectric at room temperature [30]. Application of strong electric field transforms irreversibly the relaxor state to a ferroelectric state. This is accompanied by a monoclinic (*Cc*) to rhombohedral (*R*3*c*) transformation on the global scale [31–33]. The nonergodic relaxor state of NBT is characterized by the presence of short ranged $a^0\,a^0\,c^+$ in-phase tilted octahedral regions amid $a^-a^-a^-$ tilted antiphase octahedral regions of the rhombohedral structure [34,35]. Poling suppresses the short ranged

*rajeev@iisc.ac.in

$a^0\,a^0\,c^+$ regions and system exhibits a rhombohedral structure [32]. On heating poled NBT, the in-phase tilt appears and gradually depolarizes the system in temperature interval 150−300 °C. Above 300 °C, the ferroelectric *R*3*c* distortion disappears completely; the system acquires *P*4/*mbm* tetragonal structure with $a^0\,a^0\,c^+$ tilt [36]. This phase survives up to 550 °C above which the cubic $Pm\bar{3}m$ phase sets in [37].

The $(1-x)$ST-(x)NBT alloy system offers an interesting opportunity to explore the interplay of the different types of structural-polar interactions the system inherit from both the parent compounds ST and NBT. In comparison to the analogous solid solutions like $Na_{0.5}Bi_{0.5}TiO_3$-$BaTiO_3$ (NBT-BT) [37–39] and $Na_{0.5}Bi_{0.5}TiO_3$-$K_{0.5}Bi_{0.5}TiO_3$ (NBT-KBT) [40–42], where both the end members (BT and KBT) are ferroelectric, the end member ST in NBT-ST is an incipient ferroelectric. That is, the system is susceptible to become polar when perturbed suitably. The incipience character offers scope for designing ST-based dielectric materials for high energy storage applications [43]. NBT-modified ST is among such possibilities [44]. Since, as stated above, Bi^{3+} at the *A* site of the perovskite structure promotes ferroelectric distortion, its incorporation in the ST matrix will help induce formation of polar regions and improve the polarizability even at room temperature. In this context, Yu and Ang [45] have reported that heterovalent Bi^{+3} substitution increases the unit cell volume of ST. Although the authors did not highlight this as an anomalous behavior, we may note that ionic radius of Bi^{+3} (∼1.40 Å) is smaller as compared to Sr^{+2} (1.44 Å) [46] and Bi^{+3} substitution is expected to shrink the lattice purely from the viewpoint of ionic size consideration. A plausible scenario of the lattice getting expanded, despite the smaller size Bi^{+3} ion substituting for the Sr^{+2} ion, is electrostriction. This phenomenon is associated with the formation of polar nanoregions which appear to have formed even at room temperature when Bi is incorporated into the lattice of ST. We anticipate the same phenomenon to occur when ST is alloyed with the Bi containing perovskite, NBT. However, the literature presents conflicting reports. While the data reported by Cui *et al.* [44] suggest the cell volume to decrease with increasing NBT concentration [44], a perusal of the data published by Pettry *et al.* [47] do not seem to suggest such a monotonic decrease in the volume. We may note that these studies [44,47] are not focused on structural evolution *per se*, but on the properties. The ambiguity, however, calls for a careful examination of the structural issues pertaining to the ST-NBT system. In this paper, we have explored this aspect in detail using a set of complementary tools such as neutron powder diffraction, x-ray powder diffraction, and Raman spectroscopy. In conjunction with polarization and field-driven strain measurements, we show an interesting interplay of ionic size, polar nanoregions, and octahedral tilt leading to (i) a nonmonotonic composition dependence of cell volume at room temperature and (ii) existence of a critical temperature at which the system exhibits a composition independent lattice parameter.

II. EXPERIMENT

$(1-x)SrTiO_3$-$(x)Na_{0.5}Bi_{0.5}TiO_3$ specimens were synthesized using the conventional solid state reaction method. Dried powders of $SrCO_3$ (99%, Alfa Aesar), Na_2CO_3 (99.5%, Alfa Aesar), Bi_2O_3 (99%, Alfa Aesar), and TiO_2 (99.8%, Alfa Aesar) were weighed in stoichiometric ratios and ball-milled in an acetone medium using zirconia vials and balls in a planetary ball mill at 200 rpm for 12 h. Calcination was done at 1000 °C for 4 h. The calcined powder was remilled at 200 rpm for 8 h and calcined again for better homogenization of the chemical species. Pellets of the calcined powder were made under uniaxial pressure of 250 MPa followed by the cold isostatic compaction at 350 MPa. The pellets were sintered in the range 1250–1350 °C for 6 h in ambient atmosphere. The density of the sintered pellets was ∼95%. For ferroelectric measurements the pellets (diameter of 12 mm and thickness of 0.5 mm) were painted with silver paste. X-ray powder diffraction (XRPD) patterns of the specimens were collected on powder specimens obtained by grinding the sintered pellets to powder and subsequent annealing at 700 °C for 2 h to remove the effect of residual stresses, if any, incurred during the grinding process. XRPD measurements were carried out using Rigaku SmartLab x-ray diffractometer with monochromatic Cu $K\alpha_1$ radiation, operated at 4.5 kW. Data were collected at a 2θ step size of 0.01° and scan speed of 1°/min. High temperature (in the range 30–500 °C) XRPD data were collected using the Anton Paar heating attachment with the Rigaku SmartLab diffractometer. Neutron powder diffraction (NPD) data were collected at room temperature on the Echidna diffractometer, ANSTO, using a wavelength of 1.300 Å. Structural analysis was performed by the Rietveld method using the FULLPROF software [48]. The polarization-electric field loop were taken from the Precision Premier II ferroelectric loop tester (Radiant Technologies) up to the field of 60 kV/cm at 1 Hz frequency. Raman spectra were collected using a 532-nm laser (Lab-RAM, HORIBA spectrometer) using 1 μm^2 of spot size and 50× long working distance lens. Transmission electron microscopy (TEM) examination of the samples were carried out using Titan Themis (300 keV). The TEM specimens were prepared using the conventional method, i.e., sectioning and polishing followed by ion milling to electron transparency using Gatan PIPS II.

III. RESULTS AND DISCUSSION

X-ray powder diffraction patterns of $(1-x)$ST-(x)NBT suggest a cubiclike structure for all compositions in the range $x \sim 0$−0.60 (Fig. S1 of the Supplemental Material [49]). The composition dependence of the cubic lattice parameter, however, exhibits a peculiar nonmonotonic trend with a maximum at $x \sim 0.35$ [Fig. 1(a)]. This suggests two competing processes—one that increases the volume and the other which decreases the volume. Given that the Shannon radii of Na^{+1}, Bi^{+3}, and Sr^{+2} for 12 coordination are 1.39, 1.40, and 1.44 Å [46], respectively, the average ionic radius of $(Na_{0.5}Bi_{0.5})^{+2}$ = 1.395 Å. From a pure ionic size consideration, it is therefore anticipated that the incorporation of $(Na_{0.5}Bi_{0.5})^{2+}$ into the ST matrix should decrease the unit cell volume. In contrast, the increase of lattice parameter until $x \sim 0.35$ suggests an onset of a phenomenon which expands the lattice to such an extent that it overwhelms the volume reducing tendency of the smaller sized $(Na_{0.5}Bi_{0.5})^{2+}$ ions. The trend in the lattice expansion is, however, suddenly arrested for $x > 0.35$.

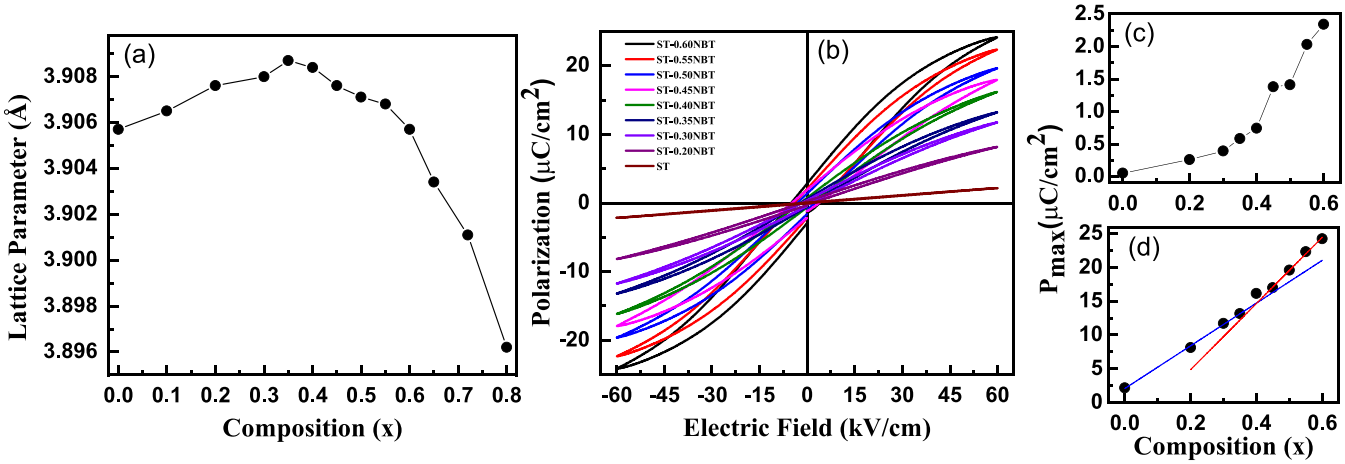

FIG. 1. (a) Composition dependence of the cubic lattice parameter of $(1-x)$ST-xNBT($x = 0.0$–0.60) (the error bars are smaller than the data points). The lattice parameter was calculated by Le-Bail fitting of PXRD data. (b) Bipolar polarization-electric field (P-E) loops at room temperature. (c) Compositional dependence of remanent polarization P_r and (d) maximum polarization P_{max} (at 60 kV/cm).

Figure 1(b) shows the polarization (P)–electric field (E) bipolar loops for the different compositions of this series. For $x = 0.00$, i.e., ST, as expected, the P-E graph is linear. Nonlinearity sets in and the P-E loop opens up gradually with the increasing NBT concentration (Fig. S2 [49]), and the unipolar strain (S)–electric field (E) loop shows an increase in hysteresis and electrostrain with composition (Fig. S3 [49]). The nonlinearity confirms the onset of polar nanoregions in the NBT modified ST specimens. The remanent polarization, which is a measure of the degree of irreversibility of the switched domains on removal of the field, shows a noticeable increase for $x > 0.35$ [Fig. 1(c)]. A similar trend was revealed in the composition dependence of the maximum polarization (measured from the bipolar P-E loops with field amplitude 60 kV/cm) which shows a notable increase in the slope of linear $P_{max} - x$ curve for $x > 0.35$ [Fig. 1(d)]. This suggest that the volume decrease for $x > 0.35$ [Fig. 1(a)] is associated with a structural distortion which promotes the development of ferroelectric correlations in the presence of strong electric field. Since the x-ray powder diffraction patterns fail to capture the structural distortion (the average structure appears to be cubic for all compositions in the range $x \sim 0$–0.60), we looked for symptoms of possible structural distortions using Raman spectroscopy, transmission electron microscopy (TEM), and neutron powder diffraction techniques.

Figure 2(a) shows the Raman spectra of $(1-x)$ST-(x)NBT. The Bose-Einstein corrected spectra were fitted with Lorentzian function to deconvolute the various vibrational Raman modes (Fig. S4 [49]). Although in principle the cubic ($Pm\bar{3}m$) symmetry of ST forbids first-order Raman modes, they are visible due to the presence of defects (strain, grain boundaries, oxygen vacancies, impurity atoms, and other external conditions [8,9]). These modes can be seen at 174, 539, and 791.4 cm^{-1} and correspond to TO_2, TO_4, and $LO_4 + A_{2g}$ modes, respectively [10,11]. Second order modes are seen in the band region of 220–500 cm^{-1} and 580–750 cm^{-1} [8,12]. With increasing NBT content, the second order scattering disappears. Defects in ST are also known to induce polar nanoregions (PNRs) which break the local inversion symmetry and contribute to the first order Raman scattering, more specifically the TO_2 and TO_4 modes [15,16]. As shown in Fig. 2(b) the intensity of both the modes increases with composition up to $x \sim 0.35$. It decreases thereafter. The similarity of this trend with the composition dependence of cell volume confirms that the volume increase in the composition range $x \sim 0$–0.35 is associated with the electrostriction caused by the growth of PNRs.

Figure S5a [49] shows the evolution of neutron powder diffraction (NPD) patterns of ST-NBT at room temperature. Similar to the XRD patterns, a cursory glance at the NPD patterns suggests a cubiclike structure for all compositions in the range $x = 0$–0.60. However, when examined carefully [Fig. 3(a)], weak superlattice peaks can be seen for compositions $x > 0.40$. On indexing with respect to a doubled cubic perovskite cell, both $\frac{1}{2}$(odd odd odd) and $\frac{1}{2}$(odd odd even) type superlattice peaks can be seen (Fig. S6 [49]). The $\frac{1}{2}$(ooo) and the $\frac{1}{2}$(ooe) type reflections are commonly attributed to the $R3c$ and $P4bm$ phases of NBT. These reflections are barely discernible for $x < 0.50$. We extracted the integrated intensities by deconvoluting the two neighbouring peaks $\frac{1}{2}$(530) and $\frac{1}{2}$(531) by fitting with two Lorentzians. From the composition evolution of the relative intensities of $\frac{1}{2}$(530) and $\frac{1}{2}$(531) peaks, shown in Fig. S5b [49], it is evident that both the $R3c$ and the $P4bm$ distortions grows simultaneously for $x > 0.35$. Our Rietveld analysis with $P4bm$+$R3c$ two phase coexistence model proved insufficient to accurately fit all the details of the NPD pattern as highlighted by the misfit regions near the superlattice reflections in Fig. S7 [49]. However, the main Bragg peaks can be fitted well (Figs. S7 and Fig. S8 [49]). A similar misfit of the superlattice peaks with $P4bm$ model has been reported in NBT-BT and NBT-KBT systems in the tetragonal phase region [37]. Following the previous reports [37,50], we label the phase as a disordered $P4bm$ phase. Our NPD study therefore confirms that the volume decrease for $x > 0.35$ is caused by the onset of octahedral tilt. Ignoring the weak superlattice peaks, the NPD patterns can be easily fitted with cubic $Pm\bar{3}m$ model. Important to note is that the composition dependence of the lattice parameter derived from the NPD data follows exactly the same trend

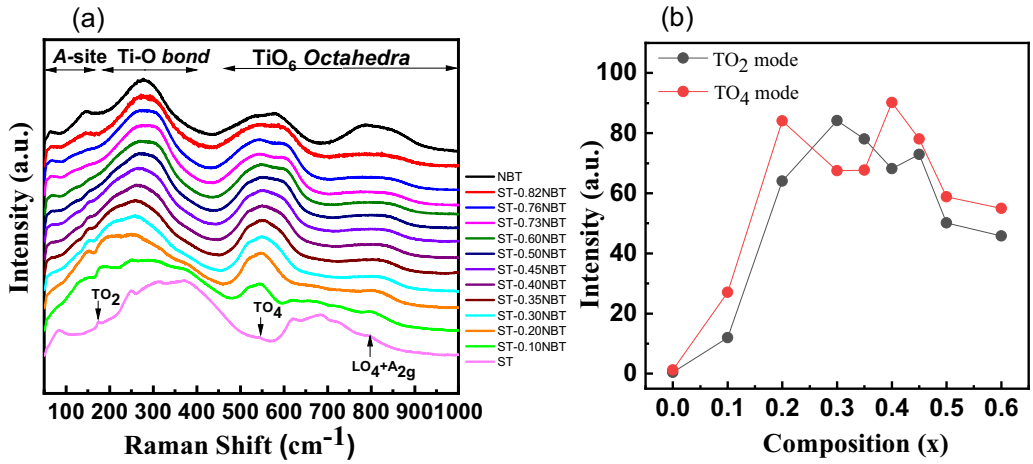

FIG. 2. (a) Raman Spectra of $(1-x)$ST-xNBT at room temperature. The data in this plot have been corrected with the Bose-Einstein factor. (b) Composition dependence of the intensity of TO_2 and TO_4 Raman modes.

as that obtained from the XRD data (Fig. S5c [49]), further confirming the correctness of the composition dependence of the lattice parameter obtained using the XRD data.

Although the NPD study suggests a correlation between octahedral tilt and a decrease in cell volume, the superlattice peaks in the NPD patterns are visible only at $x \geqslant 0.50$. On the other hand, the cell volume/lattice parameter shows a decreasing trend for $x > 0.35$, i.e., well below $x = 0.50$. To resolve this discrepancy, we performed electron diffraction studies on selected compositions $x = 0.50$, 0.30, and 0.20. Figure 3(b) depicts selected area diffraction pattern (SADP) along the [110] zone axis of $x = 0.50$. Consistent with the NPD pattern of this composition, the [110] zone axis SADP shows 1/2(odd odd odd) superlattice spots. $\frac{1}{2}$(odd odd even) superlattice spots could also be seen in the [111] zone axis SADP of this composition. Interestingly, similar diffraction spots, though with significantly less intensity, can be seen in the SADP of $x = 0.30$. In view of this, the absence of the superlattice peaks in the NPD patterns of $x = 0.30$ can be attributed to the short-range correlation of the octahedral tilt. Such a situation is not surprising in NBT-based systems. For example, 1/2{ooe) superlattice spots have been reported in the electron diffraction pattern of unpoled NBT but not in the neutron diffraction pattern, suggesting that the correlation length of the in-phase octahedral tilt is very small in NBT at room temperature [33]. The decrease of volume for $x > 0.35$ can be attributed to the onset of the octahedral tilt on the global scale. We could not detect the superlattice spots in the SADP of $x = 0.20$ confirming the absence of the octahedral tilts for this composition.

Given the contrasting influences of the octahedral tilt and ionic size *vis-à-vis* the polar nanoregions on the cell volume of ST-NBT, we sought to understand the interplay of these influences better by heating the different compositions of this

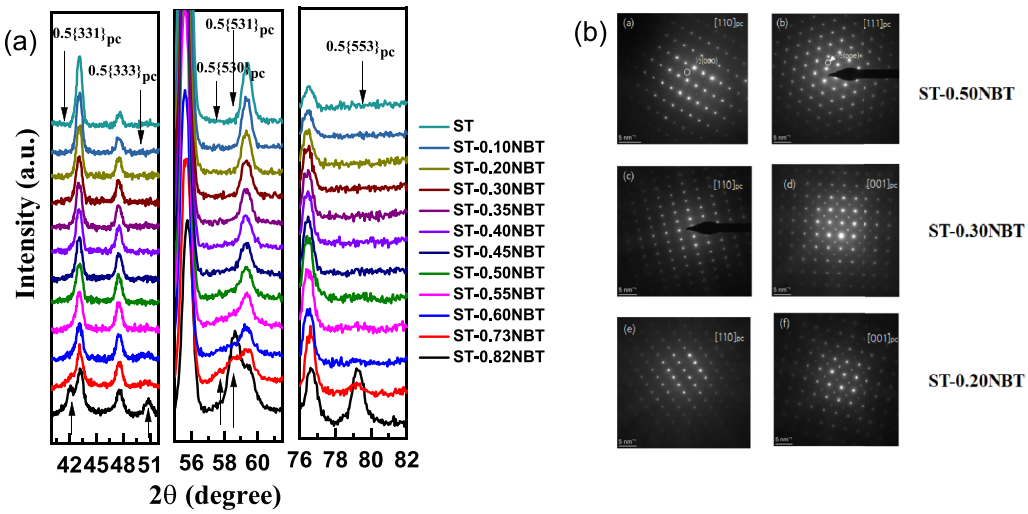

FIG. 3. (a) Parts of the neutron powder diffraction pattern of $(1-x)$ST $-$ xNBT at room temperature (the complete pattern can be seen in the Supplemental Material [49] (Fig. S3a). The superlattice peaks are indexed on the pseudocubic cell. (b) Selected area electron diffraction patterns (SADP) of ST-0.50NBT along $[110]_{pc}$ and $[111]_{pc}$ zone axes. The SADP of $x = 0.20$ and $x = 0.30$ are shown for the $[110]_{pc}$ and $[001]_{pc}$ zone axes. $x = 0.20$ does not show superstructure reflections along any of the zone axes. The composition $x = 0.30$ exhibits faint superstructure spots corresponding to $\frac{1}{2}$(ooo) and $\frac{1}{2}$(ooe) indices. Similar types of superlattice spots are also visible in the SADP of $x = 0.50$.

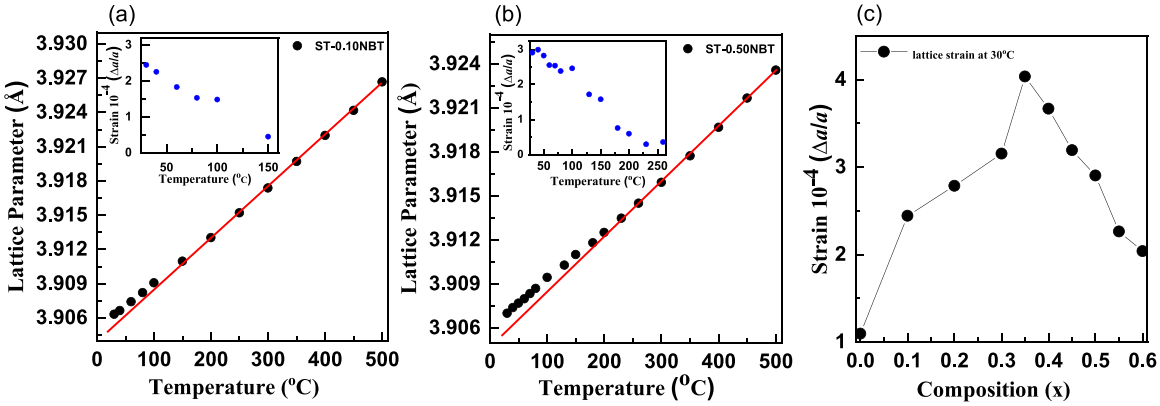

FIG. 4. Temperature evolution of the cubic lattice parameter (calculated from XRPD patterns) of two representative compositions (a) $x = 0.10$ and (b) $x = 0.50$. The solid lines are linear fit to the data in the high-temperature region. Deviations from this linear trend occur below a critical temperature. Insets depict the temperature dependence of the thermal expansion strain (calculated from the departure from linearity). (c) Composition dependence of the lattice strain at 30 °C is calculated by extrapolating a straight line from the linear region at high temperature down to room temperature, then taking the difference (Δa) of the calculated lattice parameter and the lattice parameter for the extrapolated straight line at 30 °C. The lattice strain ($\Delta a/a$) for all the compositions at room temperature is then calculated by dividing the difference by the calculated one. The nonmonotonic trend follows the intensities of the TO_2 and TO_4 Raman modes in Fig. 2(b).

system (in the range $x \sim 0-0.60$) above room temperature. The temperature evolution of the lattice parameter for a few representative compositions is shown in Figs. 4(a) and 4(b). Similar plots for the remaining compositions are shown in Fig. S9 [49]. In all cases, we found a notable departure from the linear thermal expansion behavior below a (composition dependent) critical temperature. We attribute the excess lattice parameter (with respect to the extrapolated linear trend) to electrostriction effect caused by the onset of the polar nanoregions. The excess lattice strain thus estimated at room temperature (30 °C) for the different compositions is shown in Fig. 4(c). Interestingly, this turns out to be the maximum for $x = 0.35$, i.e., the composition which also shows the maximum lattice parameter [Fig. 1(a)]. This, together with the fact that the intensity of the TO_2 and TO_4 Raman modes follow the same composition trend [Fig. 2(b)] confirms that the increase of volume with increasing composition in the range $x \sim 0-0.35$ is due to the growth of PNRs.

Figure 5(a) depicts the lattice parameter as a function of composition at different temperatures of this system. For $x < 0.40$, at room temperature, the lattice parameter increases with increasing composition. For the same composition range ($x < 0.40$), at 500 °C, the lattice parameter decreases with increasing composition. We estimated the slope da/dx at different temperatures [Fig. 5(b)] and found that there exists a temperature (~300 °C) around which the lattice parameter of this system (for $x < 0.40$) becomes independent of the composition ($da/dx = 0$). As discussed above, from the pure ionic size consideration, $Na_{0.5}Bi_{0.5}$ substitution is expected to decrease the lattice parameter. However, the electrostriction caused by the polar nanoregions dominates over the ionic size effect and expands the lattice. With increasing temperature,

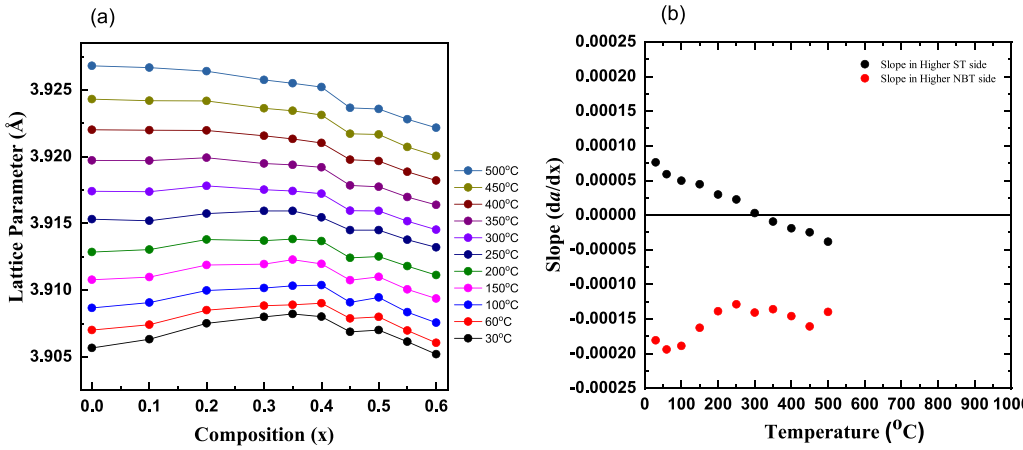

FIG. 5. (a) Composition dependence of the cubic lattice parameter (a) of $(1-x)$ST-(x)NBT at different temperatures. (b) The slope (da/dx) for the regions $x < 0.35$ and $x > 0.50$ is calculated separately at various temperatures and plotted against the temperature. The slope becomes zero at ~300 °C suggesting that at this temperature, the specimen lattice parameter is independent of the composition (in the range $x = 0-0.35$).

the polar nanoregions weaken as does their contribution to the lattice expansion. It appears that 300 °C is the temperature at which the contraction of lattice (due to ionic size) nearly compensates for the expansion due to electrostriction in the different compositions in the range $x < 0.40$, giving rise to the unusual phenomenon of composition independent lattice parameter. We may note that this feature may not be exclusive to the NBT modified ST system. More work along a similar line may reveal this interesting phenomenon in other modified ST systems.

IV. CONCLUSIONS

In conclusion, we show that the $(1 - x)$ST-(x)NBT system exhibits a complex interplay of polar nanoregions and octahedral tilt. Despite the smaller average ionic size of Na^{+1}/ Bi^{+3} with respect to Sr^{+2}, the system exhibits an anomalous increase in the lattice parameter due to dominating effect of electrostriction caused by the polar nanoregions. The onset of octahedral tilt above $x > 0.30$ reverses this trend, causing the volume to decrease with increasing x. We also show that there exists a critical temperature ∼300 °C at which the competing ionic size and electrostriction effects make the system exhibit a composition independent lattice parameter.

ACKNOWLEDGMENT

R.R. acknowledges the Science and Engineering Research Board (SERB) for financial support (Grant No. CRG/2021/000134) [50].

[1] A. D. Bruce and R. A. Cowley, Structural phase transitions III. Critical dynamics and quasi-elastic scattering, Adv. Phys. **29**, 219 (1980).

[2] K. A. Muller and H. Burkard, $SrTiO_3$: An intrinsic quantum paraelectric below 4 K, Phys. Rev. B **19**, 3593 (1979).

[3] J. H. Barrett, Dielectric constant in perovskite type crystals, Phys. Rev. **86**, 118 (1952).

[4] J. G. Bednorz and K. A. Muller, $Sr_{1-x}Ca_xTiO_3$: An XY quantum ferroelectric with transition to randomness, Phys. Rev. Lett. **52**, 2289 (1984).

[5] M. Itoh, R. Wang, Y. Inaguma, T. Yamaguchi, Y. J. Shan, and T. Nakamura, Ferroelectricity induced by oxygen isotope exchange in strontium titanate perovskite, Phys. Rev. Lett. **82**, 3540 (1999).

[6] C. Ang, Zhi Yu, P. M. Vilarinho, and J. L. Baptista, Bi:$SrTiO_3$: A quantum ferroelectric and a relaxor, Phys. Rev. B **57**, 7403 (1998).

[7] H. Unoki and T. Sakudo, Electron spin resonance of Fe^{3+} in $SrTiO_3$ with special reference to the 110°K phase transition, J. Phys. Soc. Jpn. **23**, 546 (1967).

[8] A. M. Glazer, Simple ways of determining perovskite structures, Acta Crystallogr., Sect. A **31**, 756 (1975).

[9] J. H. Haeni, P. Irvin, W. Chang, R. Uecker, P. Reiche, Y. L. Li, W. Tian S.Choudhury, M. E. Hawley, B. Craigo, A. K. Tagantsev, X. Q. Pan, S. K. Streiffer, L. Q. Chen, S. W. Kirchoefer, J. Levy, and D. G. Schlom, Room-temperature ferroelectricity in strained $SrTiO_3$, Nature (London) **430**, 758 (2004).

[10] M. E. Guzhva, V. V. Lemanov, and P. A. Markovin, Critical concentrations in Ba-doped incipient ferroelectric $SrTiO_3$, Phys. Solid State **39**, 618 (1997).

[11] V. V. Lemanov, E. P. Smirnova, and E. A. Tarakanov, Ferroelectric properties of $SrTiO_3$-$PbTiO_3$ solid solutions, Phys. Solid State **39**, 628 (1997).

[12] V. V. Lemanov, E. P. Smirnova, P. P. Syrnikov, and E. A. Tarakanov, Phase transitions and glasslike behavior in $Sr_{1-x}Ba_xTiO_3$, Phys. Rev. B **54**, 3151 (1996).

[13] D. A. Tenne, A. Soukiassian, X. X. Xi, H. Choosuwan, R. Guo, and A. S. Bhalla, Lattice dynamics in $Ba_xSr_{1-x}TiO_3$ single crystals: A Raman study, Phys. Rev. B **70**, 174302 (2004).

[14] C. Ang, J. F. Scott, Z. Yu, H. Ledbetter, and J. L. Baptista, Dielectric and ultrasonic anomalies at 16, 37, and 65 K in $SrTiO_3$, Phys. Rev. B **59**, 6661 (1999).

[15] C. Ang and Z. Yu, Phonon-coupled impurity dielectric modes in $Sr_{1-1.5x}Bi_xTiO_3$, Phys. Rev. B **61**, 11363 (2000).

[16] A. Durán, E. Martínez, J. A. Díaz, and J. M. Siqueiros, Ferroelectricity at room temperature in Pr-doped $SrTiO_3$, J. Appl. Phys. **97**, 104109 (2005).

[17] R. Garg, A. Senyshyn, H. Boysen, and R. Ranjan, Structure of the noncubic phase in the ferroelectric state of Pr-substituted $SrTiO_3$, Phys. Rev. B **79**, 144122 (2009).

[18] R. Ranjan, R. Garg, R. Hackl, A. Senyshyn, E. Schmidbauer, D. Trots, and H. Boysen, Onset of spontaneous electrostrictive strain below 520 K in Pr-doped $SrTiO_3$, Phys. Rev. B **78**, 092102 (2008).

[19] R. Ranjan, R. Hackl, A. Chandra, E. Schmidbauer, D. Trots, and H. Boysen, High-temperature relaxor ferroelectric behavior in Pr-doped $SrTiO_3$, Phys. Rev. B **76**, 224109 (2007).

[20] A. Durán, F. Morales, L. Fuentes, and J. M. Siqueiros, Specific heat anomalies at 37, 105 and 455 K in $SrTiO_3$:Pr, J. Phys.: Condens. Matter **20**, 085219 (2008).

[21] W. Kleeman and H. Schremmer, Cluster and domain-wall dynamics of ferroelectric $Sr_{1-x}Ca_xTiO_3$, Phys. Rev. B **40**, 7428 (1989).

[22] U. Bianchi, W. Kleeman, and J. G. Bednorz, Raman scattering of ferroelectric $Sr_{1-x}Ca_xTiO_3$, $x = 0.007$, J. Phys.: Condens. Matter **6**, 1229 (1994).

[23] U. Bianchi, J. Dec, W. Kleeman, and J. G. Bednorz, Cluster and domain-state dynamics of ferroelectric $Sr_{1-x}Ca_xTiO_3$ ($x = 0.007$), Phys. Rev. B **51**, 8737 (1995).

[24] J. Dec, W. Kleeman, U. Bianchi, and J. G. Bednorz, Glass-like interacting off-centre Ca^{++} dipoles as probes of the "coherent quantum state" in $SrTiO_3$, Europhys. Lett. **29**, 31 (1995).

[25] W. Kleeman, J. Dec, and B. West Wanski, Susceptibility scaling behavior of quantum paraelectric $SrTiO_3$: Ca, Phys. Rev. B **58**, 8985 (1998).

[26] R. Ranjan, D. Pandey, and N. P. Lalla, Novel features of $Sr_{1-x}Ca_xTiO_3$ phase diagram: Evidence for competing antiferroelectric and ferroelectric interactions, Phys. Rev. Lett. **84**, 3726 (2000).

[27] R. Ranjan and D. Pandey, Antiferroelectric phase transition in $(Sr_{1-x}Ca_x)$ TiO_3: II. X-ray diffraction studies, J. Phys.: Condens. Matter **13**, 4251 (2001).

[28] N. A. Hill, Why are there so few magnetic ferroelectrics? J. Phys. Chem. B **104**, 6694 (2000).

[29] A. Kumar, A. Kumar, S. Saha, H. Basumatary, and R. Ranjan, Ferromagnetism in the multiferroic alloy systems $BiFeO_3$-$Na_{0.5}Bi_{0.5}TiO_3$ and $BiFeO_3$-$SrTiO_3$: Intrinsic or extrinsic? Appl. Phys. Lett. **114**, 022902 (2019).

[30] A. R. Paterson, H. Nagata, X. Tan, J. E. Daniels, M. Hinterstein, R. Ranjan, P. B. Groszewicz, W. Jo, and J. L. Jones, Relaxor-ferroelectric transitions: Sodium bismuth titanate derivatives, MRS Bull. **43**, 600 (2018).

[31] R. Ranjan, $Na_{1/2}Bi_{1/2}TiO_3$-based lead-free piezoceramics: A review of structure-property correlation, Curr. Sci. **118**, 1507 (2020).

[32] B. N. Rao and R. Ranjan, Electric-field-driven monoclinic-to-rhombohedral transformation in $Na_{1/2}Bi_{1/2}TiO_3$, Phys. Rev. B **86**, 134103 (2012).

[33] B. N. Rao, R. Datta, S. S. Chandrashekaran, D. K. Mishra, V. Sathe, A. Senyshyn, and R. Ranjan, Local structural disorder and its influence on the average global structure and polar properties in $Na_{1/2}Bi_{1/2}TiO_3$, Phys. Rev. B **88**, 224103 (2013).

[34] I. Levin, I. M. Reaney, E.-M. Anton,W. Jo, J. Rödel, J. Pokorny, L. A. Schmitt, H.-J. Kleebe, M. Hinterstein, and J. L. Jones, Local structure, pseudosymmetry, and phase transitions in $Na_{1/2}Bi_{1/2}TiO_3$−$K_{1/2}Bi_{1/2}TiO_3$ ceramics, Phys. Rev. B **87**, 024113 (2013).

[35] V. Dorcet and G. Trolliard, A transmission electron microscopy study of the A-site disordered perovskite $Na_{0.5}Bi_{0.5}TiO_3$, Acta Mater. **56**, 1753 (2008).

[36] G. O. Jones and P. A. Thomas, Investigation of the structure and phase transitions in the novel A-site substituted distorted perovskite compound $Na_{0.5}Bi_{0.5}TiO_3$, Acta Crystallogr., Sect. B **58**, 168 (2002).

[37] G. D. Adhikary, B. Mahale, B. N. Rao, A. Senyshyn, and R. Ranjan, Depoling phenomena in $Na_{0.5}Bi_{0.5}TiO_3$ − $Na_{0.5}Bi_{0.5}TiO_3$: A structural perspective, Phys. Rev. B **103**, 184106 (2021).

[38] C. Ma, H. Guo, S. P. Beckman, and X. Tan, Creation and destruction of morphotropic phase boundaries through electrical poling: A case study of lead-free $(Bi_{1/2}Na_{1/2})TiO_3$−$Na_{0.5}Bi_{0.5}TiO_3$ piezoelectrics, Phys. Rev. Lett. **109**, 107602 (2012).

[39] K. Datta, R. B. Neder, A. Richter, M. Gobbels, J. C. Neuefeind, and B. Mihailova, Adaptive strain prompting a pseudo-morphotropic phase boundary in ferroelectric (1-x)$Na_{0.5}Bi_{0.5}TiO_3$−$xNa_{0.5}Bi_{0.5}TiO_3$, Phys. Rev. B **97**, 184101 (2018).

[40] G. D. Adhikary, D. K. Khatua, A. Senyshyn, and R. Ranjan, Random lattice strain and its relaxation towards the morphotropic phase boundary of $Na_{0.5}Bi_{0.5}TiO_3$-based piezoelectrics: Impact on the structural and ferroelectric properties, Phys. Rev. B **99**, 174112 (2019).

[41] G. D. Adhikary, D. K. Khatua, A. Senyshyn, and R. Ranjan, Long-period structural modulation on the global length scale as the characteristic feature of the morphotropic phase boundaries in the $Na_{0.5}Bi_{0.5}TiO_3$ based lead-free piezoelectrics, Acta Mater. **164**, 749 (2019).

[42] M. Otonicar, S. D. Škapin, M. Spreitzer, and D. Suvorov, Compositional range and electrical properties of the morphotropic phase boundary in the $Na_{0.5}Bi_{0.5}TiO_3$−$K_{0.5}Bi_{0.5}TiO_3$ system, J. Eur. Ceram. Soc. **30**, 971 (2010).

[43] H. Pan, F. Li, Y. Liu, Q. Zhang, M. Wang, S. Lan, Y. Zheng, J. Ma, L. Gu, Y. Shen, P. Yu, S. Zhang, L.-Q. Chen, Y.-H. Lin, and C.-W. Nan, Ultrahigh–energy density lead-free dielectric films via polymorphic nanodomain design, Science **365**, 578 (2019).

[44] C. Cui, Y. Pu, Z. Gao, J. Wan, Y. Guo, C. Hui, Y. Wang, and Y. Cui, Structure, dielectric and relaxor properties in lead-free ST-NBT ceramics for high energy storage applications, J. Alloys Compd. **711**, 319 (2017).

[45] Z. Yu and C. Ang, Crystalline structure and dielectric properties of $(Sr_{1-1.5x}Bi_x)TiO_3$ ceramics, J. Mater. Sci. **38**, 113 (2003).

[46] R. D. Shannon, Revised effective ionic radii and systematic studies of interatomic distances in halides and chalcogenides, Acta Crystallogr., Sect. A **32**, 751 (1976).

[47] J.-R. G. Pettry, S. Said, P. Marchet, and J.-P. Mercurio, Sodium-bismuth titanate based lead-free ferroelectric materials, J. Eur. Ceram. Soc. **24**, 1165 (2004).

[48] J. Rodrigues-Carvajal, *2000 FULLPROF. A Rietveld Refinement and Pattern Matching Analysis Program* (Laboratoire Leon Brillouin (CEACNRS), Saclay, France, 2000).

[49] See Supplemental Material at http://link.aps.org/supplemental/10.1103/PhysRevB.109.014107 for PXRD patterns, Neutron powder patterns, Rietveld fitted NPD patterns with refined parameter values, Unipolar S-E plots and other details.

[50] G. D. Adhikary, D. Sharma, P. Punetha, G. Jafo, G. Abebe, A. Mishra, A. Senyshyn, and R. Ranjan, Preponderant influence of disordered *P*4*bm* phase on the piezoelectricity of critical compositions of $Na_{0.5}Bi_{0.5}TiO_3$-based ferroelectrics, Phys. Rev. B **104**, 184102 (2021).